Engineering Science and Technology, an International Journal 35 (2022) 101112

HOSTED BY

Contents lists available at ScienceDirect

Engineering Science and Technology, an International Journal

journal homepage: www.elsevier.com/locate/jestch

Full Length Article

A low-profile flexible planar monopole antenna for biomedical applications

Md. Shazzadul Islam [a], S.M. Kayser Azam [b], A.K.M. Zakir Hossain [c,*], Muhammad I. Ibrahimy [a], S.M.A. Motakabber [a]

[a] Department of Electrical and Computer Engineering, International Islamic University Malaysia, Jalan Gombak 53100, Selangor, Malaysia
[b] Department of Electrical Engineering, University of Malaya, 50603 Kuala Lumpur, Malaysia
[c] Centre for Telecommunication Research & Innovation, Fakulti Teknologi Kejuruteraan Elektrik & Elektronik, Universiti Teknikal Malaysia Melaka, Jalan Hang Tuah Jaya, Durian Tunggal, Melaka, Malaysia

ARTICLE INFO

Article history:
Received 9 July 2021
Revised 30 December 2021
Accepted 3 February 2022

Keywords:
Flexible antenna
X-band frequency
In-Vivo test
Figure of merit
Biomedical application

ABSTRACT

This article proposes a low profile planar monopole antenna on flexible substrate. The antenna is designed with an elliptical slot inserted in a rectangular patch by utilizing the coplanar waveguide (CPW) feeding technique on a polyimide substrate. The proposed antenna operates within 7–14 GHz ($S_{11} < -10$ dB) with a minimum return loss is observed as low as – 58 dB by simulation, whereas the entire X-band is covered by the – 20 dB bandwidth while maintaining an excellent VSWR of almost 1. Also, the antenna exhibits an average gain of 4 dBi while the average radiation efficiency is 92%. The maximum SAR of the proposed antenna for 1 g mass is below 1.0 W/Kg throughout the entire bandwidth. To observe flexibility, four different bending conditions of the antenna have been analyzed. For experimentation, the antenna has been realized as a prototype by using a low-cost fabrication process. The measurement reveals that the prototype has a −10 dB bandwidth of 5.4 GHz. During In-Vivo test, over the variation of $0 \sim 3$ mm distance between the antenna-prototype and the human chest/chicken breast tissue, the best performance is obtained at 3 mm in terms of the return loss. One of the significant features of the proposed design is its measured average and peak gain of 4.4 dBi and of 6.33 dBi respectively with a measured average efficiency of 65%. The proposed antenna has a compact size of 13×13 mm^2 ($0.35\lambda_g \times 0.35\lambda_g$), and its performance remains nominally constant even under different bending conditions which makes the antenna suitable for biomedical imaging applications. A new figure-of-merit has been introduced to evaluate the overall performance based on different antenna key parameters. The fabricated antenna would contribute to the future biomedical research by utilizing X-band frequencies.

1. Introduction

Antennas are mostly employed as fundamental components in wireless communication systems as it is the front-end device of it. It plays vital role for transmitting and receiving electromagnetic wave in free space. The modern communication system shows different us of antenna for different applications rather than only for communication purpose like, portable wireless device [1,2], radar application [3], biomedical application [4] and so on. Throughout the recent time, antennas are widely used for different biomedical applications in two different ways - either implanted in human body or placed on the body surface e.g. biomedical imaging [5,6]. To deal with the concern in human health while avoiding expensive devices for medical diagnosis, antennas are employed for biomedical Electromagnetic Imaging (EMI) in Microwave and Millimeter-wave (mm-wave) frequencies where imaging systems mostly depend on the antenna-sensor and its operating bandwidth. In EMI, the electromagnetic (EM) wave is transmitted from an antenna which travels through the medium of interest and received by another antenna (for bi-static) or antennas (for multi-static) on the other side.

When the travelling wave passes through an object in the medium of different dielectric properties, a change occurs in the wave-response. In biological objects, such phenomenon happens because of discontinuities in dielectric properties of biological tissues. Incident-waves scatter back and backscattered-waves are collected by a receiving antenna or antennas. Thus, observing the received signal responses due to different dielectric properties between

* Corresponding author.
E-mail address: zakir@utem.edu.my (A.K.M. Zakir Hossain).
Peer review under responsibility of Karabuk University.

https://doi.org/10.1016/j.jestch.2022.101112
2215-0986/

the normal and the malignant tissue is the basic concept of the biomedical EMI.

Unlike the conventional X-ray mammography that requires ionizing radiation and uncomfortable compression, non-ionizing radiation is utilized by Microwave Imaging (MWI) for Brest Cancer Detection (BCD). Also, MWI requires less expensive devices than that of the other two conventional techniques (MRI and ultrasound echograph). In overall, MWI is harmless, portable and accessible with transmitters and receivers based on low-cost components [7]. Several research works related to the microwave imaging for breast cancer detection have been presented in [6,8–12]. Mostly, S-band and C-band have been utilized by MWI systems for BCD. In [6], an 18 × 18 mm^2 monopole antenna designed on a flexible Polyimide substrate has been utilized by constructing an antenna array of 16 elements to perform a multi-static radar imaging for BCD. With the same monopole antenna, a wearable prototype (wearable medical-bra) embedded with 16 elements antenna array has been proposed in [8]. The imaging system has been proposed for S-band frequency with a 2 GHz operating bandwidth. However, no electromagnetic performance is reported except the antenna geometry. While in [9], a flexible monopole antenna has been proposed for BCD at C-band frequencies to embed with wearable medical-bra. The proposed antenna has achieved 2 GHz (4 – 6 GHz) operating bandwidth with a minimum return loss of −27 dB, an average gain of 1 dBi and an average radiation efficiency of 70%. Since in lower microwave frequencies, it is easy to penetrate highly dense fatty tissues of the breast, this frequency range is mostly utilized by breast cancer imaging techniques. Also, the image resolution depends on the operating bandwidth and working frequency ranges of MWI systems. Whereas, in previously described works, the operating bandwidth of proposed MWI systems is only 2 GHz. On the other hand, MWI systems with wide operating bandwidth in the higher frequency range can result in high-resolution images. Therefore, some researchers have proposed MWI systems for BCD with high profile travelling-wave Vivaldi antennas of wide-bandwidth in ultra-wideband (UWB) frequencies [10–12]. For example, a directive-featured side slotted Vivaldi antenna (SSVA) has been proposed for BCD with size reduction and gain improvement features in [10]. The return loss of the proposed antenna is found as −38 dB at 4.4 GHz with a wide −10 dB bandwidth of around 5.25 GHz (3.9 – 9.15 GHz). An average gain of the antenna is 4.9 dBi with an average radiation efficiency of 88%. However, there is a noticeable lack of gain flatness over the entire bandwidth although the antenna occupies a small area of 45 × 37 mm^2. With the same design method, another SSVA antenna has been proposed to improve antenna performance for BCD in [11]. An increase of 2 dBi in the gain, 250 MHz in the bandwidth and 4% in the efficiency have been achieved at the cost of a large antenna dimension of 88 × 75 mm^2. To reduce this additional dimension, a balanced slotted antipodal Vivaldi antenna (BSAVA) has been designed on 40 × 40 mm^2 FR-4 substrate in [12]. The antenna bandwidth has been increased to 8 GHz (2.5 GHz more) while antenna gain, and efficiency have been decreased to 5 dBi and 75% respectively. In fact, Vivaldi antennas are suitable for monostatic and bi-static MWI systems due to their bandwidth, gain and efficiency. However, their rigid and voluminous structures make them less suitable for multi-static MWI systems for BCD. Recently, a CPW-fed antenna has been proposed in [13] for bi-static MWI systems. Although the antenna has a bandwidth of 4.5 GHz with an average gain of 5 dBi and radiation efficiency of 82%, its large dimension of 76 × 44 mm^2 makes it unsuitable for a multi-static MWI that require multiple compact antennas to create high resolution images.

For early breast cancer-detections, image resolutions are increased in the higher frequency-range because the wavelength becomes shorter. This provides an extra advantage in contemporary biomedical applications by utilizing mm-wave imaging (mm-WI) techniques [14]. As a result, no deep skin-penetration is required by the cancer margins detection during the surgical removal in [15], corneal hydration sensing in [16], dental diagnosis and treatment in [17], and early skin cancer detection in [18]. In fact, mm-WI for BCD is possible since breast cancer imaging (BCI) concepts for different frequencies like mm-wave, THz and even infrared frequency spectrum are already introduced [19–21]. Yet, dielectric characterizations of the breast tissues are available up to 20 GHz and more than 150 GHz [22–25]. Therefore, in [26], the dielectric properties of the malignant and healthy breast-tissues have been characterized for 0.5 – 50 GHz. Accordingly, in [27], a breast cancer imaging system with a bandwidth of 13.5 GHz (26.5 – 40 GHz) is proposed by employing the WR28 waveguide to excite the array of 32 flexible antennas. An array of 32 flexible antennas have been used; but no information about the geometry, parameters or performances of the antenna has been reported. Therefore, a printable monopole antenna on flexible substrate has been proposed in [28]. Where, the proposed antenna has achieved – 10 dB bandwidth of 18.7 GHz, operates from 21 GHz to 39.7 GHz. The antenna has a compact size of 5 × 5 mm^2 in the area with an average antenna gain of 4 dBi and antenna efficiency of more than 80%. However, the system requires expensive components-based transmitters, receivers and RF switch-matrixes (for multi-static BCI). Meanwhile, the X-band frequency spectrum can be an optimized selection for electromagnetic BCI in terms of low-cost wearable devices for biomedical and futuristic 5G applications. Like in [29], a flexible inkjet-printed monopole wideband antenna (7 – 13 GHz) has been recently proposed for 5G communication. Despite the antenna has an average gain of 5 dBi, it has a poor efficiency of 31% and a large dimension of 60 × 75 mm^2 on a flexible Polyethylene Terephthalate (PET) substrate. Another flexible antenna with a small size of 36 × 32 mm^2 and a decent efficiency of 62% has been proposed for skin cancer identification in [30] by maintaining an average gain of 1.4 dBi over its 4 GHz bandwidth. Although flexible antennas struggle with gain and radiation-efficiency compared to non-flexible antennas, modern biomedical applications need flexible antennas to perform satisfactorily at different bending conditions. Thus, some major challenges remain in flexible antenna design for biomedical applications by making a suitable trade-off among different parameters.

In this article, a very low-profile flexible planar monopole antenna has been proposed for biomedical applications. Besides, a new Figure of Merit has been introduced to assess the overall antenna performance. The proposed antenna has been designed on a flexible 125μ m thin Polyimide substrate that operates from 7 GHz to 14 GHz. The dielectric constant and loss tangent of the substrate are 3.5 and 0.0027, respectively. The antenna is compact and has a quasi-omnidirectional radiation pattern that offers freedom of placing the antenna in both ways on the body surface from the front and the back.

2. Antenna development

2.1. Antenna synthesis

Unlike the conventional Rectangular Ring Slotted Planar Monopole Antenna (RRSPMA) and Circular Ring Slotted Planar Monopole Antenna (CRSPMA) as shown in Fig. 1(a) and Fig. 1(b), respectively, the proposed antenna is designed with an elliptical slot by following the hierarchical step as illustrated in Fig. 2.

Although RRSPMA and CRSPMA typically have wideband characteristics on rigid substrates, these conventional designs still have limitations in improving the overall antenna performances on flexible substrates. Thus, in this work, a parasitic slot other than those

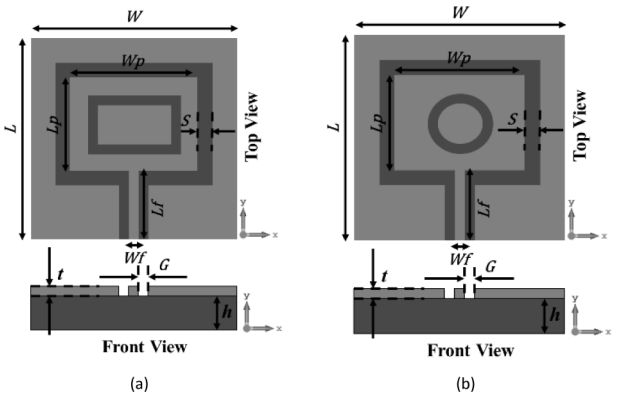

Fig. 1. Conventional designs (**a**) RRSPMA, (**b**) CRSPMA.

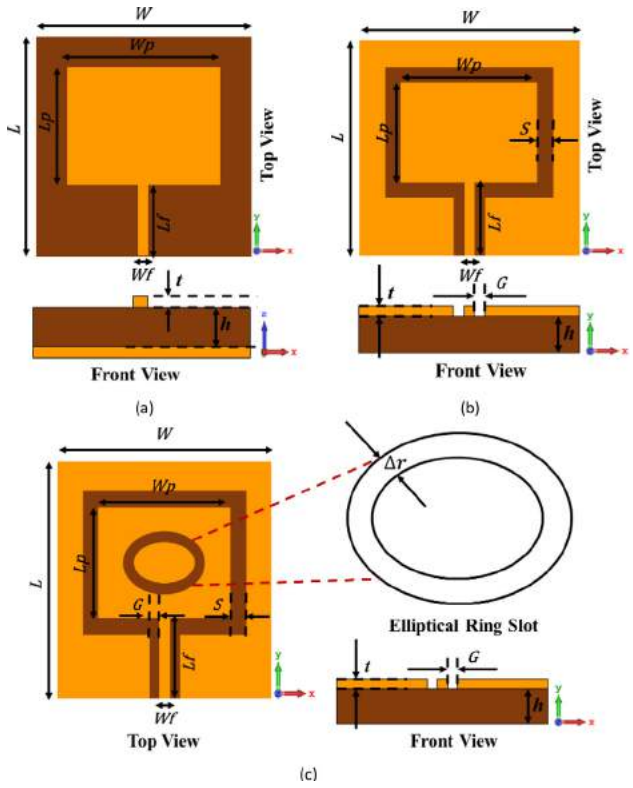

Fig. 2. *Antennas design steps and geometry.* (**a**) MRPA, (**b**) PMA and (**c**) proposed ERSPMA.

conventional shapes is designed though a hierarchical design procedure. At first, a conventional Microstrip Rectangular Patch Antenna (MRPA) is designed which typically has a narrow bandwidth. To convert the MRPA into a wideband antenna, a Planar Monopole Antenna (PMA) is designed by removing the ground plane from the MRPA and a new ground plane has been designed on the same plane (top plane) with the radiating patch by adopting the CPW feeding technique as shown in Fig. 2. Geometrical design of the conventional MRPA and PMA antennas are shown in Fig. 2(a) and Fig. 2(b), respectively. As depicted in Fig. 2(b), two rectangular-shaped ground planes have been designed with a gap (G) from both sides of the feedline, and then both ground planes have been connected by surrounding the radiating patch with the spacing (S) between the patch and the ground to make a symmetrical and common ground-line. For the ERSPMA geometry shown in Fig. 2 (c), the inner radius for the x-axis, $r_{in}(x)$ = 2 mm and for y-axis, $r_{in}(y)$ = 1.5 mm, and the outer radius for the x-axis, $r_{out}(x)$ = 2.5 mm and for y-axis, $r_{in}(y)$ = 2 mm. Thus, the slot width is equally maintained by 0.5 mm throughout the ERS geometry. In same directions, the slot width is denoted as $\Delta r = (r_{out} - r_{in})$ to ease the further discussion. These hierarchical designs are based on flexible Kapton Polyimide films with a dielectric thickness (h) of 0.125 mm and a dielectric constant (ε_r) of 3.5 for the resonant frequency (f_r) at 10 GHz that is also the center frequency of the X-band. Rectangular patch dimensions (patch width,W_p and patch length, L_p), and microstrip feedline width (W_f) are calculated by utilizing antenna design formulae [31,32] with CST Microwave Studio (MWS).

The space (S) between the patch and the ground plays a vital role in controlling the bandwidth as shown in Fig. 3(a). With the increase of S, bandwidth of the antenna decreases. On the other hand, Δr of the ERS significantly improves the impedance matching of the antenna as shown in Fig. 3(b). Thus, bandwidth and impedance matching of the antenna are controllable by the proposed design without making any change in the gap G and the length of elliptical circumference. As observed from Fig. 3, there are two resonant frequencies of the proposed ERSPMA. From the theoretical perspective, these two resonant frequencies of the proposed ERSPMA can be approximated by the modified equation (1) and (2) for the first and second resonance, respectively [33], since the lower and the upper resonance points are controlled by the width of the patch (w_p) and the inner circumference of the elliptical slot (C_e), respectively.

$$f_{r1} \approx \frac{\vartheta_0}{2w_p}\sqrt{\frac{1}{\varepsilon_r + 2}} \tag{1}$$

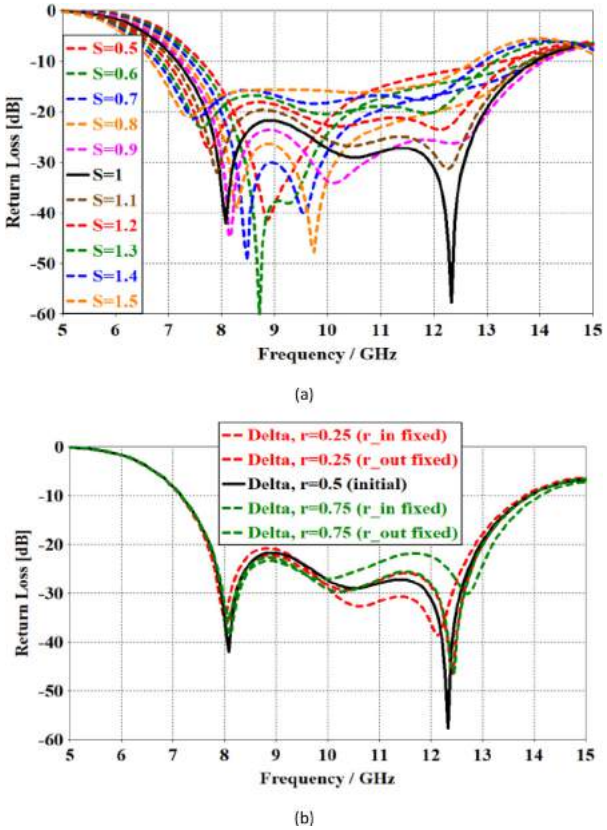

Fig. 3. *Effects with the changes of S and Δr on the proposed ERSPMA* ***(a)****S and* ***(b)*** *Δr.*

$$f_{r2} \approx \frac{\vartheta_0}{C_e\sqrt{\varepsilon_r + 1}} \tag{2}$$

$$C_e \cong 4(a+b)\left(\frac{\pi}{4}\right)^{\frac{4ab}{(a+b)^2}} \tag{3}$$

Here, the circumference of ellipse is approximated by (3) [34] as the ϑ_0 denotes the speed of light for free space.

Since the ERSPMA is symmetrically constructed, capacitances due to the electric gap-coupling are symmetrically distributed throughout the ERSPMA. Although the capacitance due to any space, gap or slot of a CPW-fed antenna is weakly formed by the effective dielectric properties of air and the antenna substrate, yet it has significant contributions to the overall antenna performance depending on the antenna design technique. Based on the proposed technique, the ERSPMA is designed and optimized by using CST MWS. Parametrically, the proposed design performs stably on different flexible substrates within a range of thicknesses (h) from 50μ m to 250μ m and dielectric constants (ε_r) from 2.3 to 3.5. As per Fig. 4, the ERSPMA is designed on three substrates of different thicknesses and dielectric properties. Corresponding dimensions of the proposed ERSPMA on three different substrates are given in Table 1.

A multilayer human tissue-mimicking breast phantom is designed by CST MWS to calculate the average specific absorption rate (ASAR) as illustrated in Fig. 5. Relative permittivity and conductivity of the tissue are extracted for 7–14 GHz [35] while the mass density is reported in [6] for different breast tissues. Physical parameters of the simulated breast model are provided in Table 2.

2.2. ERSPMA analysis

Based on the antenna performance simulated in CST MWS, the ERSPMA has achieved improved results compare to the PMA, RRSPMA and CRSPMA that can be observed form return loss (S11) and VSWR as comprised in Fig. 6. The PMA has achieved a minimum return loss of – 33 dB, while, the ERSPMA has achieved as low as – 58 dB. There is a decrease of 25 dB has been achieved with deep sharp notch with the ERS o the radiating patch that also leads a good impedance matching of the ERSPMA as seen in Fig. 6 (b). Whereas RRSPMA and CRSPMA have achieved minimum return loss of – 10 dB and – 4 dB respectively with the RRS and CRS on the radiating patch. In fact, both RRSPMA and CRSPMA have poor impedance matching as seen in Fig. 6(b). From the analyses in Fig. 6, it is obvious that the proposed ERSPMA design is more stable than that of the conventional PMA in terms of their impedance matching.

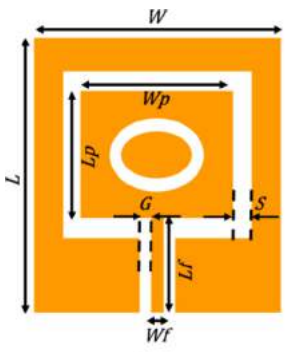

(a)

Name	ε_r	δ	h
Polyimide	3.5	0.0027	125
Paper	2.31	~0.06	231
PET	3.2	0.02	100

(b)

Fig. 4. *ERSPMA **(a)** final design **(b)** substrate specifications.*

Table 1
ERSPMA dimensions on different substrates.

Parameters in mm (λ_g)	Polyimide	Paper	PET
W	13 (0.65)	13 (0.55)	13 (0.65)
L	13 (0.65)	13 (0.55)	13 (0.65)
W_p	8 (0.4)	8 (0.33)	8 (0.4)
L_p	6 (0.3)	6.5 (0.27)	6 (0.3)
W_f	0.28	0.6	0.2
L_f	4.7	3.6	4.7
G	0.4	0.5	0.4
S	1	1	1
h	0.125	0.230	0.100

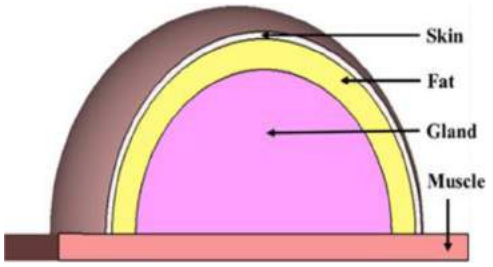

Fig. 5. Human tissue-mimicking breast phantom.

Stability in impedance matching is further observed from return loss (S11) and VSWR of the proposed ERSPMA on three different substrates as shown in Fig. 7.

In case of Paper and PET, bandwidths are found similar as ERSPMA on Polyimide substrate. However, ERSPMA on Polyimide offers more stable response than other two. In fact, the entire X-band is covered by return loss lower than – 20 dB by the proposed ERSPMA both on Polyimide and PET substrates. On Paper substrate, the X-band is covered by the return loss lower than – 15 dB of the ERSPMA. Hence, ERSPMA offers stable impedance matching that is also justified by its minimum VSWR value (close to 1 within X-band) for all three substrates. Significance of the ERS can be visualized from the surface current distribution on the radiating patch. On Polyimide substrate, as shown in Fig. 8, surface current is more accumulated on the radiating patch of the ERSPMA (435 A/m) than that of PMA (173 A/m), RRSPMA (123 A/m) and CRSPMA (132 A/m).

Increase of surface current in the radiating patch and stability in impedance matching of the ERSPMA improve the antenna gain and radiation efficiency as shown in Fig. 9. In fact, peak gain is increased by 0.4 dBi and average gain is increased by 0.75 dBi from PMA to ERSPMA. Peak gain and average gain of the ERSPMA are 4.2 dBi and 3.95 dBi respectively, whereas peak gain and average gain of the PMA are 3.8 dBi and 3.2 dBi, and both RRSPMA and CRSPMA have average gain of 3.7 dBi with peak gain of 4 dBi.

The average radiation efficiency of the PMA and ERSPMA are 85% and 92% respectively. Because of the good impedance matching and accumulated surface current on the radiating patch, an increase of 7% in the average radiation efficiency has achieved with the ERS on patch. However, the RRSPMA and CRSPMA have very low average efficiency of 56% and 44% with maximum radiation efficiency of 82% and 58% respectively. Meanwhile, there is a decrease of 29% and 41% radiation efficiency with the RRS and CRS on the patch respectively than that of PMA. A comparison of antenna gain and radiation efficiency is shown in Fig. 10 for ERSPMA on three substrates where flat-gain characteristics are observed over the entire X-band.

Table 2
ERSPMA dimensions on different substrates.

Tissue	Skin	Fat	Gland	Muscle
Thickness (mm)	2	8	120	8
Inner radius (mm)	68	60	0	0
Outer radius (mm)	70	68	60	0
Mass Density (Kg/m3)	1010	928	1035	1040

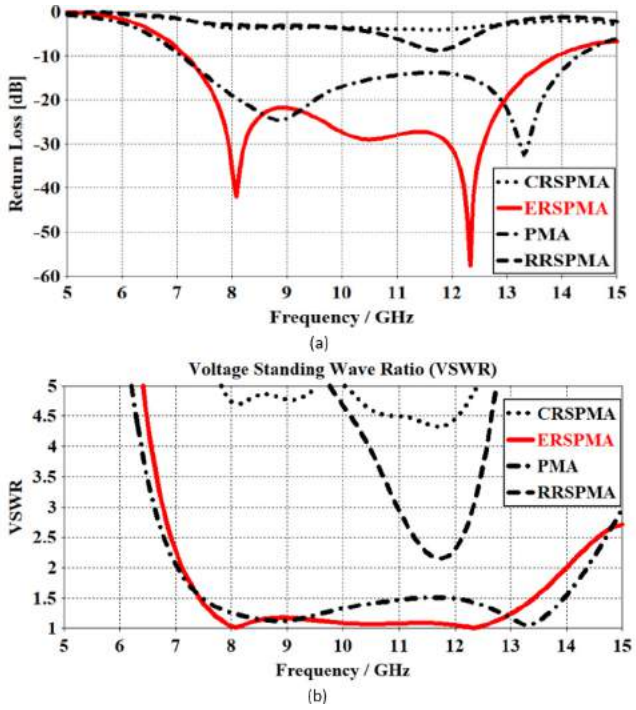

Fig. 6. Performance analysis of PMA, RRSPMA, CRSPMA and ERSPMA **(a)** return loss **(b)** VSWR.

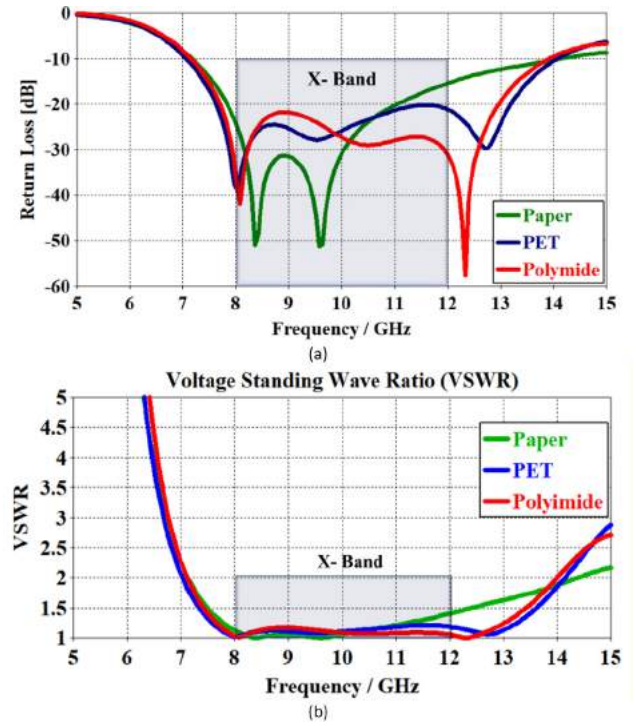

Fig. 7. ERSPMA analysis **(a)** return loss **(b)** VSWR.

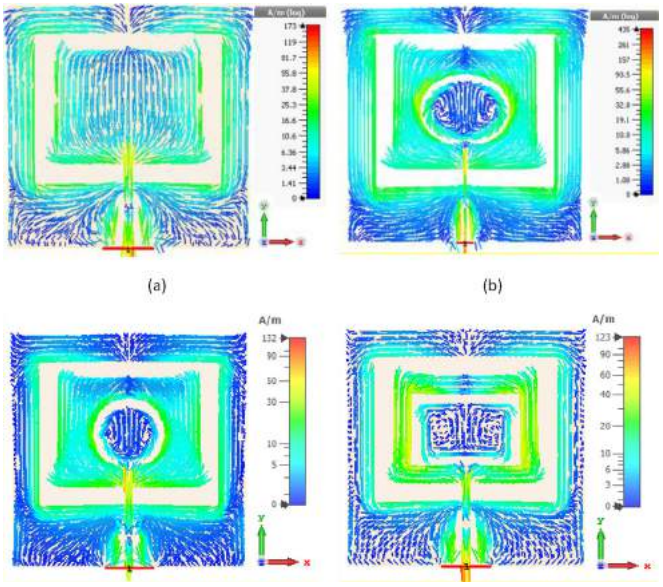

Fig. 8. Surface current at 10 GHz **(a)** PMA **(b)** ERSPMA **(c)** CRSPMA and **(d)** RRSPMA.

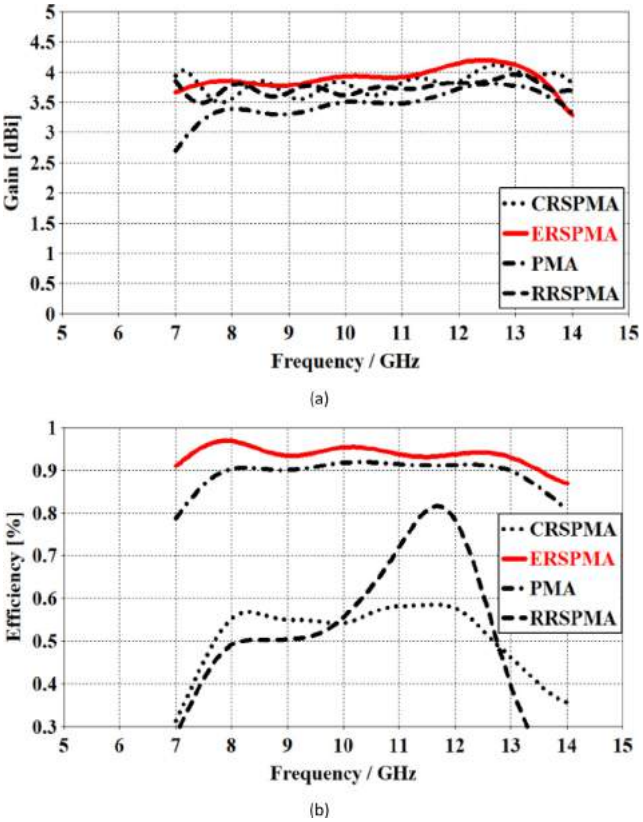

Fig. 9. Performance analysis of PMA, RRSPMA, CRSPMA and ERSPMA **(a)** gain **(b)** efficiency.

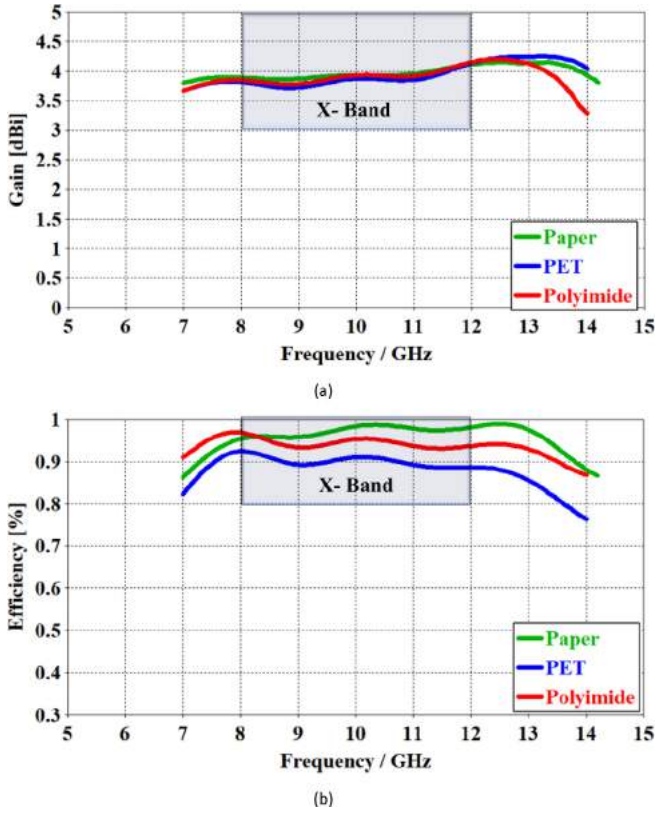

Fig. 10. ERSPMA analysis **(a)** gain **(b)** efficiency.

Peak gain of 4.2 dBi, 4.15 dBi and 4.25 dBi are obtained by the ERSPMA respectively for Polyimide, Paper and PET substrates. An average efficiency of 92 % over the antenna bandwidth and 95% over the X-band are found for ERSPMA on Polyimide substrate. Compared to PMA, the ERSPMA has 7% and 4% more antenna efficiency for the antenna bandwidth and smart bandwidth (X-band) respectively. However, because of the low loss characteristic of the material, ERSPMA on Paper substrate has achieved highest efficiency compared to the ERSPMA on Polyimide and PET substrate. On three substrates, ERSPMA has achieved an average efficiency above 85% with a quasi-omnidirectional radiation pattern.

The polar (linear omnidirectional cut) and 3D radiation pattern of the ERSPMA have been illustrated in Fig. 11. It is clearly visible that the level of cross polarization is least for the antenna on Polyimide substrate than others while cross polarization is found highest on Paper substrate. Paper substrate is not suitable for biomedical applications like breast cancer imaging. Again, ERSPMA on PET substrate exhibits low radiation efficiency. Thus, further analysis of the ERSPMA is presented only for the Polyimide substrate. Radiation pattern (Polar and 3D) of ERSPMA on the polyimide substrate over the human tissue-mimicking 3D breast phantom is shown at the bottom of Fig. 11. It is seen from the pattern that radiated power of the antenna is slightly reflected due to the material dissimilarities. However, the penetration of power still continues to work because of the dielectric properties of the biomaterials. This phenomenon will be more obvious while observing the SAR distribution to the breast model. The average antenna efficiency is more than 40% and maximum efficiency is around 50% while the antenna is placed on the phantom.

A multilayer breast tissue phantom is designed in CST MWS. The SAR distribution in the breast model is illustrated in Fig. 12 (a). The maximum SAR over the model is found way below 1.6 W/Kg for 1 g body model (IEEE C95. 1–1999 standard) as shown

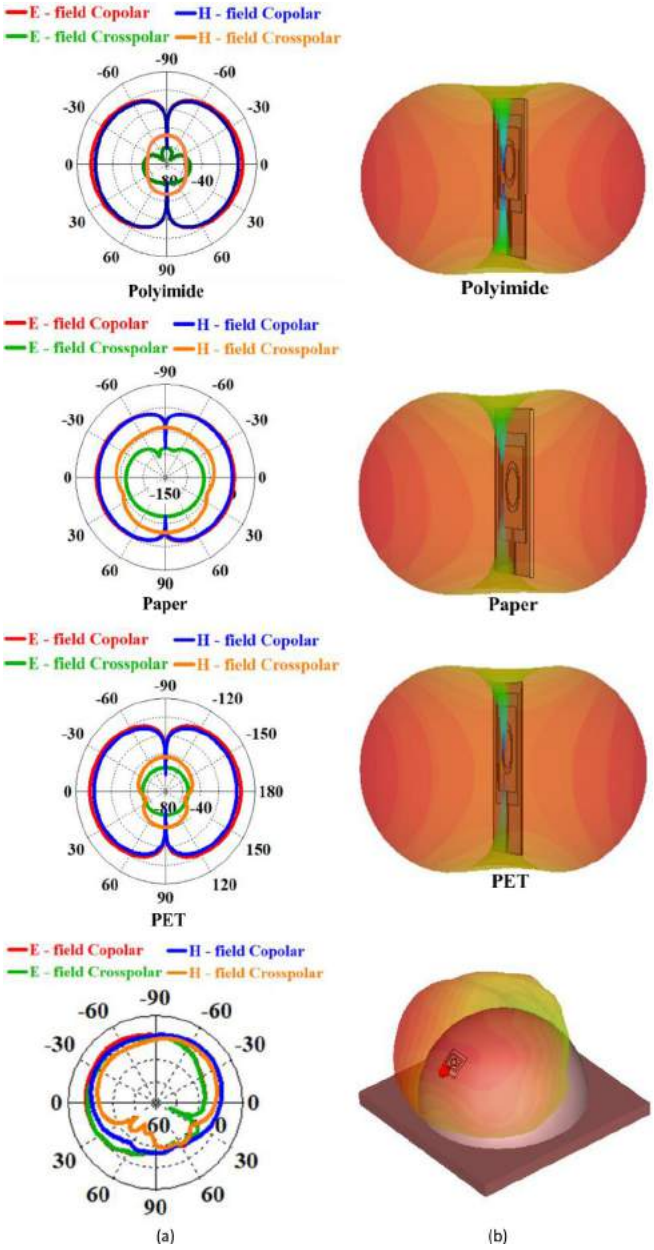

Fig. 11. Radiation pattern at 10 GHz **(a)** polar **(b)** 3D.

in Fig. 12(b). With different distance (d) from 0 to 3 mm between the antenna and the breast tissue model, the maximum SAR is approximately found as 1 W/Kg for 1 g tissue-mimicking phantom. The input power used in the SAR simulation is 0.5 W.

The average cup size for middle-aged women is from 50 mm to 70 mm. Therefore, the proposed ERSPMA antenna has been bent in the radius between 50 mm and 70 mm with steps of 5 mm in four different ways i.e. XZ-plane Downward, XZ-plane Upward, YZ-plane Downward and YZ-plane Upward. The bending effects on the antenna parameters are carried out in terms of return loss, antenna gain and radiation pattern. Return losses of the antenna at four different bending conditions is stable enough as observed from Fig. 13.

While bending along XZ- plane upward and downward, a little change in the minimum return loss and bandwidth is found. On the other hand, while bending along YZ-plane upward and downward, some frequent changes in the antenna frequency and bandwidth

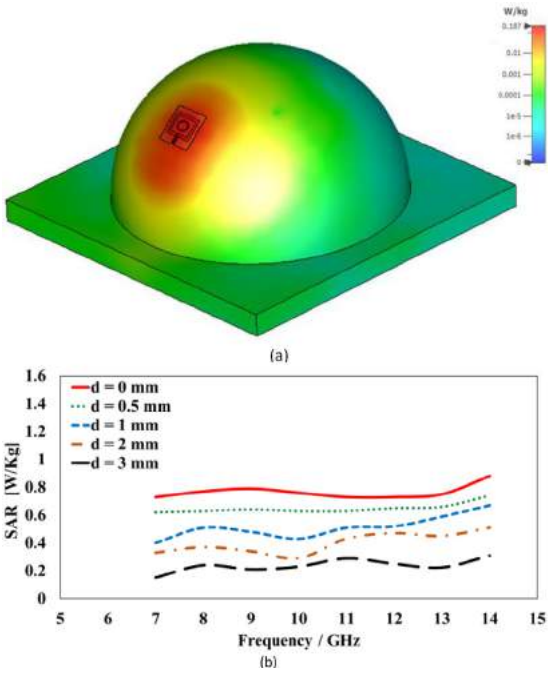

Fig. 12. (**a**) ERSPMA with breast phantom with 3 mm distance (**b**) maximum SAR for different distances.

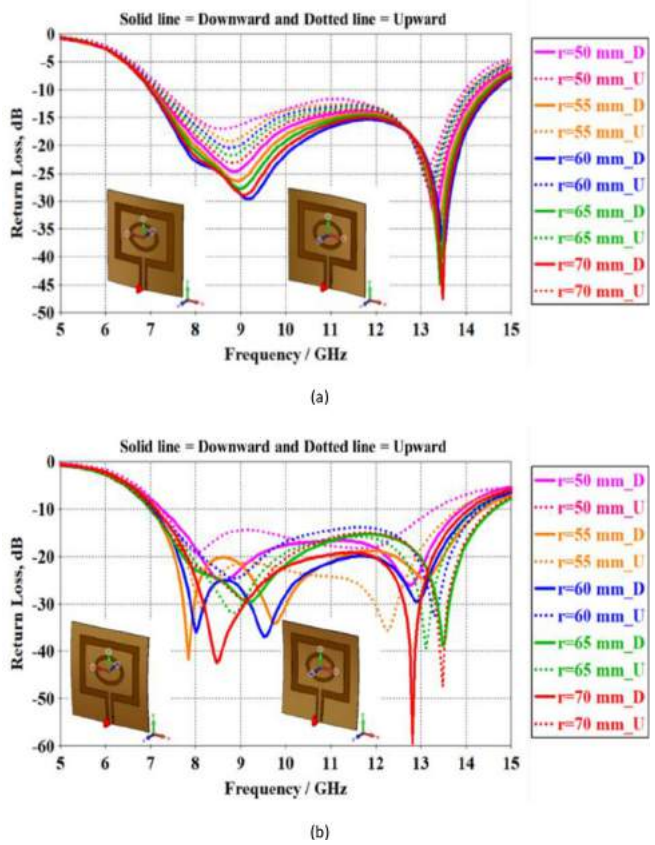

Fig. 13. Return loss of ERSPMA with bending (**a**) XZ-plane (**b**) YZ-plane.

are observed in terms of the return loss. Nevertheless, the – 10 dB bandwidth covers the entire 7 GHz bandwidth for all cases except for the bending along YZ-plane upward for the radius 50 mm and 55 mm. In fact, if the antenna is bent more, its performances decrease at a negligible level. Meanwhile, the peak antenna gain is increased at the bending conditions as shown in Fig. 14. For the bending along XZ-plane and YZ-plane, the antenna peak gain reaches around 5 dBi and 4.8 dBi respectively at around 10.5 GHz which is the middle frequency of the bandwidth (7 – 14 GHz) for all four conditions.

The radiated power is distributed uniformly for the entire bandwidth at the normal condition. However, in bending conditions, the radiated power is accumulated around the bending axis at the center frequency of the bandwidth. This can be better understood by observing the radiation pattern from Fig. 15 while the antenna is bent. It is found that the radiation pattern is dented while the antenna is bent. Both the e-field and h-field of the proposed ERSPMA is dented because the radiating power concentrates around the bending axis. However, even in bending conditions, the antenna works efficiently with similar radiation patterns of normal conditions.

2.3. Prototype fabrication

Although the design is primarily considered for fabrication by using the inkjet printing on a flexible substrate with silver/copper nanoparticle conductive ink, such a fabrication process is not easily available and the ink itself is expensive. To ensure low-profile attributes in the fabrication process, an optimized prototype has been developed by the widely available etching process. For the precise resolution in the etching process, only the feedline of the proposed antenna has been optimized from 0.28 mm to 0.50 mm while other dimensions are unchanged. It is so because the etching process is performed to the conductive tape pasted on a flexible substrate which may encounter a risk of feedline decay due to the over-

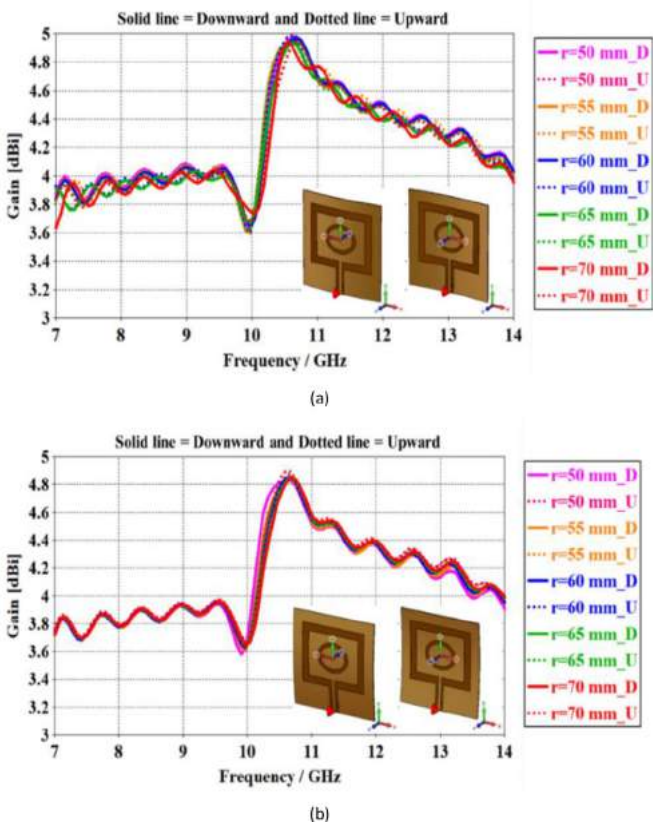

Fig. 14. Antenna gain of ERSPMA with bending (**a**) XZ-plane (**b**) YZ-plane.

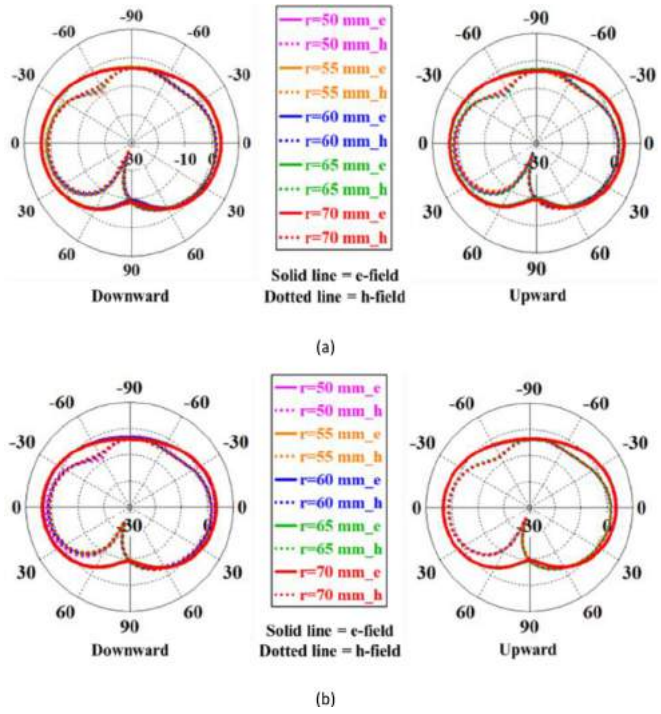

Fig. 15. Radiation pattern of ERSPMA with bending **(a)** XZ-plane **(b)** YZ-plane.

reaction in chemical process. The prototype fabrication process is briefly shown in Fig. 16.

The optimized design is printed on a single-sided glossy paper (on the glossy side) by a laser printer. A copper tape is pasted on the polyimide Kapton film to make the one-sided copper-cladding flexible polyimide substrate. Then, the printed design is transferred on the Polyimide substrate by a heat-press machine. The transferred design on the substrate is etched by a chemical solution of Hydrogen Peroxide (6% w/v) and Acetic Acid with a quantity ratio of 1:2. The etching is done by keeping the transferred design drowned into the chemical solution for about 1.5 h to remove bare coppers. As polyimide films can sustain temperature over 400 ^{0}C, an SMA port is soldered to attach the CPW-feeding.

3. Experimental results and performance Evaluation:

3.1. Experimental results

The developed prototype has been measured for its practical performances. Return loss (S_{11}), VSWR, antenna gain, and radiation pattern have been measured by using Keysight E5071C ENA VNA, N9020A MXA Signal Analyzer, horn-antenna and anechoic chamber as in Fig. 17.

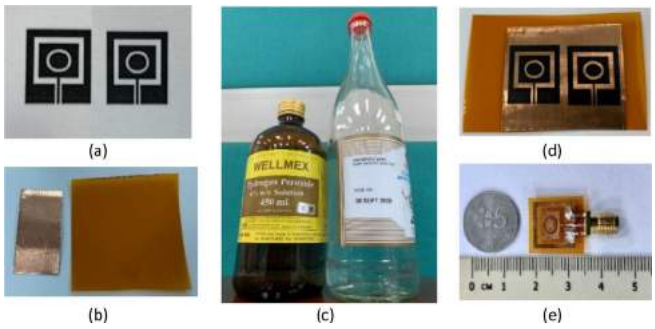

Fig. 16. *Prototype Fabrication **(a)** printed design **(b)** copper tape and polyimide Kapton film **(c)** chemical ingredients **(d)** transferred design **(e)** final prototype.*

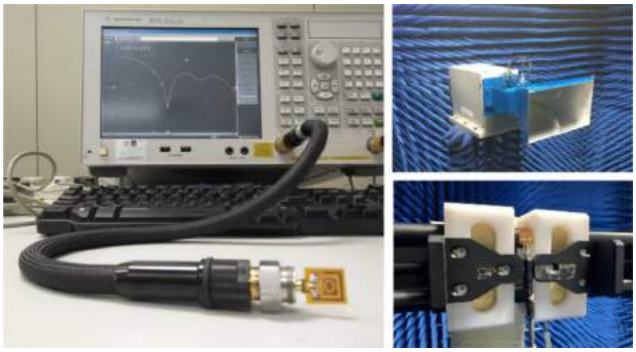

Fig. 17. Measurement setup and experimental environment.

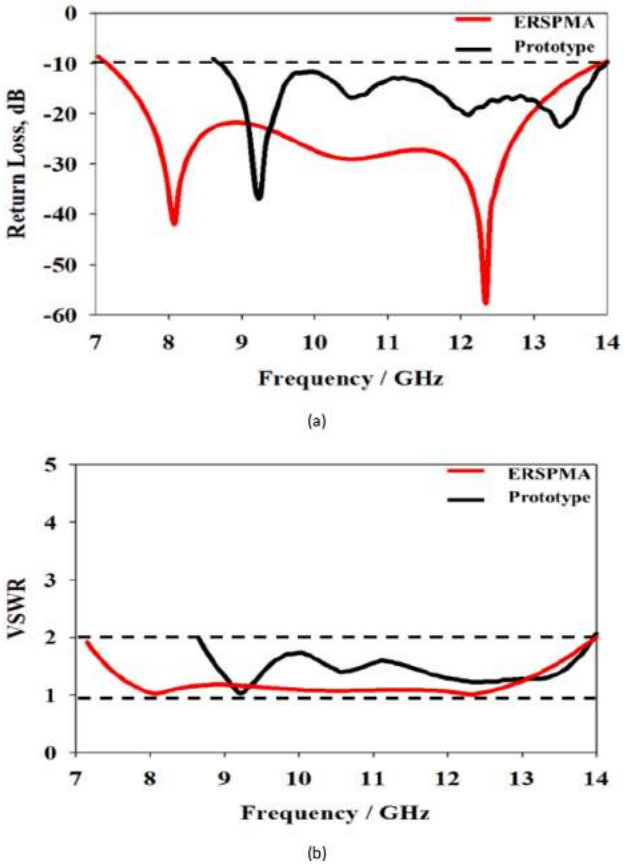

Fig. 18. Measurement results **(a)** return loss **(b)** VSWR.

Measured return loss and VSWR are presented in Fig. 18. The developed prototype offers a – 10 dB bandwidth from 8.6 GHz to 14 GHz with minimum return loss below – 37 dB. Bandwidth is decreased due to the fabrication process as discussed in section 2.2. Due to the manual fabrication of the proposed antenna as in Fig. 16, there were some deformities around the rectangular patch that controls the first resonant frequency. As a result, there is a slight change in the antenna bandwidth for the fabricated prototype. Yet, the second resonant frequency is not much affected by the manual fabrication. However, it can be forecasted from the trend of measurement results that the proposed antenna with a better fabrication will overcome this issue. Nevertheless, the

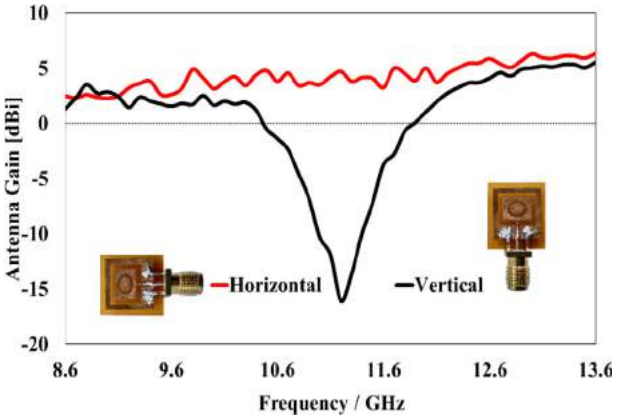

Fig. 19. Antenna gain for the vertical and horizontal position.

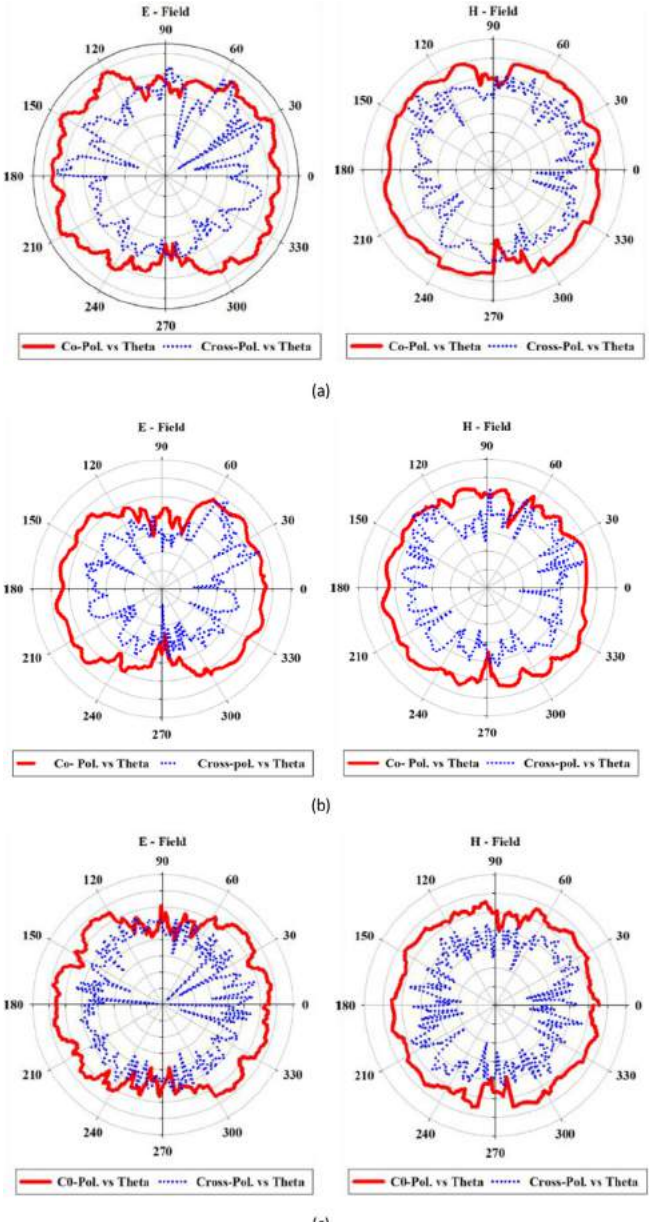

Fig. 20. Radiation pattern of the prototype (within laboratory scale) at **(a)** 8.6 GHz **(b)** 10 GHz **(c)** 12 GHz.

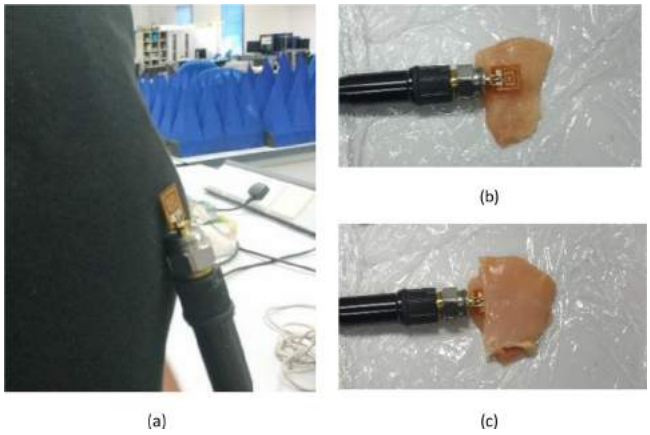

Fig. 21. In-Vivo measurement setup **(a)** with Human chest **(b)** on Chicken breast and **(c)** inside Chicken breast.

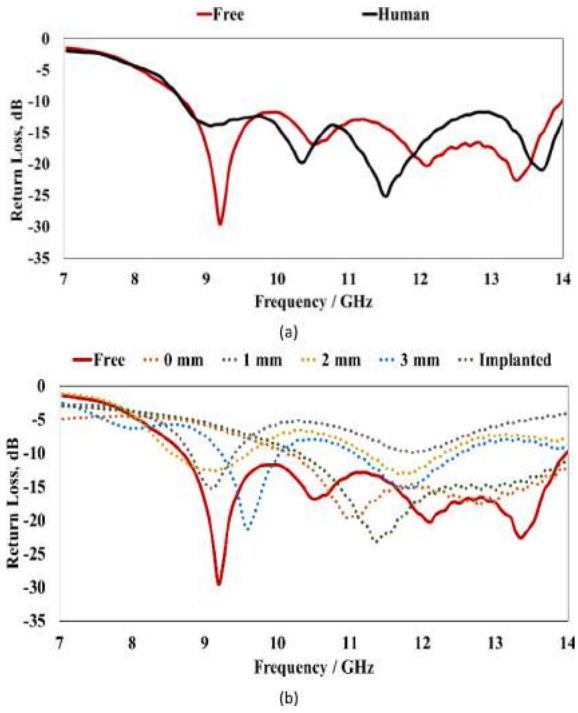

Fig. 22. Measured return loss of the prototype **(a)** with Human chest and **(b)** with Chicken breast.

antenna has a wide bandwidth with a minimum VSWR (close to 1) that validates its stable impedance matching characteristics.

Within the capacity of signal generator, measured gain of the antenna prototype is presented in Fig. 19.

The measured radiation patterns at three different frequencies of the X-band are presented in Fig. 20. A typical omnidirectional radiation pattern is generated at the H-plane (azimuth) for planar monopole antenna. Radiated power can drop of zero at the E-plane (zenith) with the change in the elevation angle which exactly happens with the prototype. The antenna prototype offers an average flat gain of 4.4 dBi and a peak gain of 6.33 dBi in the horizontal position. The main-lobe directions are at 0^0 and 180^0 as expected for lower frequencies despite some ripples are found in higher frequencies due to the fabrication error. However, these ripples are expected to be removed by fabricating the antenna by ink-jet

Table 3
Comparative evaluation of antenna performances.

Ref.	Antenna Type	Flexible	Size L × W (mm^2)	A_g (λ_g^2)	Range (GHz)	FBW (%)	G_A (dBi)	η_{RA} (%)	GoA (dBi/λ_g^2)	FoM_A(dB)
[4]	Monopole	No	6 ×8.8	0.29 × 0.43 (approx.)	2–12	143	–	56 (Array)	–	–
[9]	Monopole	Yes	24 × 14	0.40 × 0.25	4 to 6	40	1	70	10	−30
[13]	Monopole	No	76 × 44	0.89 × 0.52	3.1 to 7.6	84	5	82	10.8	−34.28
[29]	Monopole	Yes	60 × 75	1.25 × 1.00	7 to 13	60	5	31	4	−49.72
[30]	Monopole	Yes	36 × 32	1.20 × 1.01	8 to 12	40	1.4	62	1.15	−48.34
[37]	Monopole	Yes	58 ×40	1.52 × 1.05	4.1–4.3	4.76	3.6	–	2.26	–
[38]	Monopole	Yes	30 × 30	0.63 × 0.63	3.4–7.2	71	5	–	12.6	–
[39]	Monopole	Yes	30 × 30	1.09 × 1.09	5.71–5.99	4.8	3.08	80.5	2.6	−51.67
This Work	**Monopole (Prototype)**	**Yes**	**13 × 13**	**0.35 × 0.35**	**8.6 to 14**	**48**	**4.4**	**65**	**35.92**	**−37.38**

printing. Yet, in terms of E-plane and H-pane co-polarization, both meet a good agreement.

In-Vivo test has been carried out to evaluate the antenna performances. Therefore, the return loss measurement of the developed prototype has been done with a chicken breast and Human chest. The measurement setup and measured return loss of the proposed antenna have shown in Fig. 21 and Fig. 22, respectively.

The return loss of the developed prototype shows good agreement with the Human body as presented in Fig. 22(a). In both cases (Free and with Human Chest), the – 10 dB bandwidth covers from 8.6 GHz to 14 GHz with the distance of 3 mm between the antenna and the Human skin. Fig. 22(b) shows that the antenna return loss in three different positions like in Free space, on the Chicken breast tissue with four different distances (0, 1, 2 and 3 mm), and inside the Chicken breast tissue (Implanted). Closer the antenna to the bio-tissue interaction, more the antenna performance degrades due to the dielectric lossy characteristic of the bio-tissue. According to the In-Vivo test, it is found that the antenna-prototype exhibits its best performance from 3 mm distance with both Human chest and Chicken breast tissue.

3.2. Performance evaluation

Particular parameters i.e., fractional bandwidth, average gain, radiation efficiency, physical dimensions etc. determine the overall performance of an antenna. The average gain over physical aperture area is one way of evaluating the antenna performance as Gain over Area (GoA),

$$GoA = G_A/A_g \tag{4}$$

Here, G_A is the average realized gain (in terms of peak realized gain), and A_g is the physical aperture area (in terms of the guided wavelength,λ_g). However, the evaluation in (4), other parameters i.e., average radiation efficiency, fractional bandwidth, wavelength etc. are absent. Again, from [36], realized gain is found as,

$$G_A = \frac{4\pi \times A_g}{{\lambda_0}^2} \times \left(1 - |\Gamma|^2\right) \tag{5}$$

Here, Γ is the reflection coefficient which becomes negligible when peak realized gain is achieved. In that case, if the realized gain of an antenna is considered as the first index (X_1) of performance assessment, then (5) can be expressed as follow,

$$X_1 = \frac{4\pi \times A_g}{{\lambda_0}^2} \tag{6}$$

It is evident from (6) that increasing the physical aperture area enhances the gain, whereas, increasing the wavelength (or decreasing the frequency) decreases the gain. On the other hand, for any specific applications like biomedical imaging, increasing the fractional bandwidth improves the antenna performance. Nevertheless, an antenna with wideband characteristics can still fail to improve its overall performance if the radiation efficiency decreases. Thus, the product of average radiation efficiency (η_{RA}) and fractional bandwidth (FBW) is considered as the second index (X_2) of performance assessment,

$$X_2 = \frac{\eta_{RA} \times FBW}{100\% \times 100\%} \tag{7}$$

As expressed in (7), for the same FBW, one antenna performs better than the other by increasing the η_{RA}. Similarly, for the same η_{RA}, one antenna performs better than the other if the FBW is increased. Now, by combining (6) and (7), a unified Figure of Merit (FoM_A) is obtained to represent a common quantifying term of assessing the overall antenna performance,

$$FoM_A = 10 \times \log_{10}\left(\frac{X_2}{X_1}\right) \tag{8}$$

As a result, from (8), for a particular application, different antennas can be compared for their common parameters through the following formula,

$$FoM_A = 10 \times \log_{10}\left[\left(\frac{\eta_{RA} \times FBW}{100\% \times 100\%}\right) / \left(\frac{4\pi \times A_g}{{\lambda_0}^2}\right)\right] \tag{9}$$

Following the discussion above, it is obvious that the overall performance of an antenna improves when the Figure of Merit (FoM_A) in (9) is increased. Therefore, while each antenna parameter used here has its individual significance, to compare the overall performance of different antennas for their common application, FoM_A in (9) can be utilized and verified only for planar types. For the biomedical application, the developed prototype of the proposed ERSPMA is compared with some of the most relevant works as presented in Table 3.

4. Conclusion

A new flexible antenna with wide bandwidth, high gain and high efficiency has been proposed for biomedical applications in X-band frequencies. The proposed printable ERSPMA offers a wide bandwidth of 7 GHz that operates from 7 GHz to 14 GHz with a minimum return loss of – 58 dB and a minimum VSWR of nearly 1. The proposed antenna exhibits stable operating bandwidth while working on three different flexible substrates. More than 4 dBi average gain with over 92% radiation efficiency for all three substrates have been achieved by the proposed design. Moreover, the antenna shows stable performances while bending it along four different directions. An optimized prototype of the proposed antenna has been implemented by utilizing the low-cost manufacturing process. Within the laboratory scale, the measurement results show that the antenna prototype offers a wide bandwidth of 5.4 GHz with a minimum return loss of – 37 dB and a minimum

VSWR of nearly 1. The measured average gain of the antenna prototype is 4.4 dBi while the peak gain is found as 6.33 dBi. Performances of the proposed antenna can be further increased by implementing it through ink-jet printing. The proposed antenna has a quasi-omnidirectional radiation pattern that allows it to be placed on the body surface both with front and back positions. In-Vivo test exhibits suitable performances with Human and Chicken Breast tissues. Thus, the antenna is applicable for low-cost biomedical imaging systems. The proposed antenna occupies a compact area of 13×13 mm^2 on a flexible material which makes it suitable for utilizing in implantable systems and wearable garments for different biomedical applications.

Declaration of Competing Interest

The authors declare that they have no known competing financial interests or personal relationships that could have appeared to influence the work reported in this paper.

Acknowledgments

This work was accomplished by a collaboration between the Fakulti Teknologi Kejuruteraan Elektrikal dan Elektronik (FTKEE) at the Universiti Teknikal Malaysia Melaka (UTeM) and the Department of Electrical and Computer Engineering (ECE) at the International Islamic University Malaysia (IIUM). This work was funded by the Ministry of Higher Education (MOHE) through Fundamental Research Grant Scheme (FRGS) with grant reference No. FRGS/1/2021/TK0/UTEM/02/34.

References

[1] M. Alibakhshi-Kenari, M. Naser-Moghadasi, R.A. Sadeghzadeh, B.S. Virdee, E. Limiti, A new planar broadband antenna based on meandered line loops for portable wireless communication devices, Radio Sci. 51 (7) (2016) 1109–1117, https://doi.org/10.1002/2016RS005973.

[2] M. Alibakhshikenari, B.S. Virdee, E. Limiti, Compact Single-Layer Traveling-Wave Antenna DesignUsing Metamaterial Transmission Lines, Radio Sci. 52 (12) (2017) 1510–1521, https://doi.org/10.1002/2017RS006313.

[3] S. Palanivel Rajan, C. Vivek, Analysis and Design of Microstrip Patch Antenna for Radar Communication, J. Electr. Eng. Technol. 14 (2) (2019) 923–929, https://doi.org/10.1007/s42835-018-00072-y.

[4] M. Alibakhshikenari, B.S. Virdee, P. Shukla, N.O. Parchin, L. Azpilicueta, C.H. See, R.A. Abd-Alhameed, F. Falcone, I. Huynen, T.A. Denidni, E. Limiti, Metamaterial-Inspired Antenna Array for Application in Microwave Breast Imaging Systems for Tumor Detection, IEEE Access 8 (2020) 174667–174678, https://doi.org/10.1109/ACCESS.2020.3025672.

[5] A.T. Mobashsher, K.S. Bialkowski, A.M. Abbosh, S. Crozier, X. Zhang, Design and Experimental Evaluation of a Non-Invasive Microwave Head Imaging System for Intracranial Haemorrhage Detection, PLoS ONE 11 (4) (2016) e0152351, https://doi.org/10.1371/journal.pone.0152351.

[6] H. Bahramiabarghouei, E. Porter, A. Santorelli, B. Gosselin, M. Popovic, L.A. Rusch, Flexible 16 Antenna Array for Microwave Breast Cancer Detection, IEEE Trans. Biomed. Eng. 62 (10) (2015) 2516–2525, https://doi.org/10.1109/TBME.2015.2434956.

[7] N. Nikolova, Microwave Imaging for Breast Cancer, IEEE Microwave Mag. 12 (7) (2011) 78–94, https://doi.org/10.1109/MMM.2011.942702.

[8] E. Porter, H. Bahrami, A. Santorelli, B. Gosselin, L.A. Rusch, M. Popovic, A Wearable Microwave Antenna Array for Time-Domain Breast Tumor Screening, IEEE Trans. Med. Imaging 35 (6) (2016) 1501–1509, https://doi.org/10.1109/TMI.2016.2518489.

[9] A. Rahman, M.T. Islam, M.J. Singh, S. Kibria, M. Akhtaruzzaman, Electromagnetic Performances Analysis of an Ultra-wideband and Flexible Material Antenna in Microwave Breast Imaging: To Implement A Wearable Medical Bra, Sci. Rep. 6 (2016) 38906, https://doi.org/10.1038/srep38906.

[10] M.Z. Mahmud, M.T. Islam, M. Samsuzzaman, S. Kibria, N. Misran, Design and parametric investigation of directional antenna for microwave imaging application, IET Microwaves Antennas Propag. 11 (6) (2017) 770–778, https://doi.org/10.1049/iet-map.2016.0774.

[11] M.T. Islam, M.Z. Mahmud, N. Misran, J. Takada, M. Cho, Microwave Breast Phantom Measurement System With Compact Side Slotted Directional Antenna, IEEE Access 5 (2017) 5321–5330, https://doi.org/10.1109/ACCESS.2017.2690671.

[12] M.T. Islam, M. Samsuzzaman, M.T. Islam, S. Kibria, M.J. Singh, A Homogeneous Breast Phantom Measurement System with an Improved Modified Microwave Imaging Antenna Sensor, Sensors. 18 (2018) 2962, https://doi.org/10.3390/s18092962.

[13] M.Z. Mahmud, M.T. Islam, N. Misran, S. Kibria, M.d. Samsuzzaman, Microwave Imaging for Breast Tumor Detection Using Uniplanar AMC Based CPW-Fed Microstrip Antenna, IEEE Access 6 (2018) 44763–44775, https://doi.org/10.1109/ACCESS.2018.2859434.

[14] F. Topfer, J. Oberhammer, Millimeter-Wave Tissue Diagnosis: The Most Promising Fields for Medical Applications, IEEE Microwave Mag. 16 (4) (2015) 97–113, https://doi.org/10.1109/MMM.2015.2394020.

[15] A.J. Fitzgerald, V.P. Wallace, M. Jimenez-Linan, L. Bobrow, R.J. Pye, A.D. Purushotham, D.D. Arnone, Terahertz Pulsed Imaging of Human Breast Tumors, Radiology 239 (2) (2006) 533–540, https://doi.org/10.1148/radiol.2392041315.

[16] D.B. Bennett, Z.D. Taylor, P. Tewari, S. Sung, A. Maccabi, R.S. Singh, M.O. Culjat, W.S.G. M.d, J.-P. Hubschman, E.R. Brown, Assessment of corneal hydration sensing in the terahertz band: *in vivo* results at 100 GHz, JBO. 17 (2012) 097008. https://doi.org/10.1117/1.JBO.17.9.097008.

[17] Y. Nikawa, N. Hoshi, K. Kawai, S. Ebisu, Study on dental diagnosis and treatment using millimeter waves, IEEE Trans. Microw. Theory Tech. 48 (2000) 1783–1788, https://doi.org/10.1109/22.883854.

[18] A. Taeb, S. Gigoyan, S. Safavi-Naeini, Millimetre-wave waveguide reflectometers for early detection of skin cancer, IET Microwaves Antennas Propag. 7 (14) (2013) 1182–1186, https://doi.org/10.1049/iet-map.2013.0189.

[19] S. Moscato, G. Matrone, M. Pasian, A. Mazzanti, M. Bozzi, L. Perregrini, F. Svelto, G. Magenes, P. Arcioni, P. Summers, A mm-Wave 2D Ultra-Wideband Imaging Radar for Breast Cancer Detection, Int. J. Antennas Propag. 2013 (2013) 1–8, https://doi.org/10.1155/2013/475375.

[20] S.J. Erickson-Bhatt, M. Roman, J. Gonzalez, A. Nunez, R. Kiszonas, C. Lopez-Penalver, A. Godavarty, Noninvasive surface imaging of breast cancer in humans using a hand-held optical imager, Biomed. Phys. Eng. Express 1 (4) (2015) 045001, https://doi.org/10.1088/2057-1976/1/4/045001.

[21] C. Yu, S. Fan, Y. Sun, E. Pickwell-MacPherson, The potential of terahertz imaging for cancer diagnosis: A review of investigations to date, Quant Imaging Med Surg. 2 (2012) 33–45, https://doi.org/10.3978/j.issn.2223-4292.2012.01.04.

[22] M. Lazebnik, D. Popovic, L. McCartney, C.B. Watkins, M.J. Lindstrom, J. Harter, S. Sewall, T. Ogilvie, A. Magliocco, T.M. Breslin, W. Temple, D. Mew, J.H. Booske, M. Okoniewski, S.C. Hagness, A large-scale study of the ultrawideband microwave dielectric properties of normal, benign and malignant breast tissues obtained from cancer surgeries, Phys. Med. Biol. 52 (20) (2007) 6093–6115, https://doi.org/10.1088/0031-9155/52/20/002.

[23] M. Lazebnik, L. McCartney, D. Popovic, C.B. Watkins, M.J. Lindstrom, J. Harter, S. Sewall, A. Magliocco, J.H. Booske, M. Okoniewski, S.C. Hagness, A large-scale study of the ultrawideband microwave dielectric properties of normal breast tissue obtained from reduction surgeries, Phys. Med. Biol. 52 (10) (2007) 2637–2656, https://doi.org/10.1088/0031-9155/52/10/001.

[24] P.C. Ashworth, E. Pickwell-MacPherson, E. Provenzano, S.E. Pinder, A.D. Purushotham, M. Pepper, V.P. Wallace, Terahertz pulsed spectroscopy of freshly excised human breast cancer, Opt. Express, OE. 17 (2009) 12444–12454, https://doi.org/10.1364/OE.17.012444.

[25] B.C.Q. Truong, H.D. Tuan, A.J. Fitzgerald, V.P. Wallace, H.T. Nguyen, A Dielectric Model of Human Breast Tissue in Terahertz Regime, IEEE Trans. Biomed. Eng. 62 (2) (2015) 699–707, https://doi.org/10.1109/TBME.2014.2364025.

[26] A. Martellosio, M. Bellomi, M. Pasian, M. Bozzi, L. Perregrini, A. Mazzanti, F. Svelto, P.E. Summers, G. Renne, L. Preda, Dielectric Properties Characterization From 0.5 to 50 GHz of Breast Cancer Tissues, IEEE Trans. Microw. Theory Tech. 65 (3) (2017) 998–1011, https://doi.org/10.1109/TMTT.2016.2631162.

[27] S. Di Meo, F. Svelto, P.E. Summers, G. Renne, L. Preda, M. Bellomi, P.F. Espin-Lopez, A. Martellosio, M. Pasian, G. Matrone, M. Bozzi, G. Magenes, A. Mazzanti, L. Perregrini, On the Feasibility of Breast Cancer Imaging Systems at Millimeter-Waves Frequencies, IEEE Trans. Microw. Theory Tech. 65 (5) (2017) 1795–1806, https://doi.org/10.1109/TMTT.2017.2672938.

[28] M.S. Islam, M.I. Ibrahimy, S.M.A. Motakabber, A.K.M.Z. Hossain, S.M.K. Azam, A wideband millimeter-wave printable antenna on flexible substrate for breast cancer imaging, in: Putrajaya, 2019. http://www.iium.edu.my/icom/programme.pdf (accessed December 23, 2019).

[29] M. Tighezza, S.K.A. Rahim, M.T. Islam, Flexible wideband antenna for 5G applications, Microwave Opt. Technol. Lett. 60 (1) (2018) 38–44, https://doi.org/10.1002/mop.30906.

[30] A. Mersani, L. Osman, J.-M. Ribero, Flexible UWB AMC Antenna for Early Stage Skin Cancer Identification, Prog. Electromagn. Res. 80 (2019) 71–81, https://doi.org/10.2528/PIERM18121404.

[31] M.S. Islam, M.I. Ibrahimy, S.M.A. Motakabber, A.K.M.Z. Hossain, A Rectangular Inset-Fed Patch Antenna with Defected Ground Structure for ISM Band, in: 2018 7th International Conference on Computer and Communication Engineering (ICCCE), 2018, pp. 104–108, https://doi.org/10.1109/ICCCE.2018.8539260.

[32] M.S. Islam, M.I. Ibrahimy, S.M.A. Motakabber, A.K.M.Z. Hossain, S.M.K. Azam, Microstrip patch antenna with defected ground structure for biomedical application, Bull. Electr. Eng. Inf. 8 (2019) 586–595, https://doi.org/10.11591/eei.v8i2.1495.

[33] A. Sharma, P. Khanna, K. Shinghal, A. Kumar, Design of CPW-Fed Antenna with Defected Substrate for Wideband Applications, J. Electr. Comput. Eng. 2016 (2016) 1–10, https://doi.org/10.1155/2016/6546481.

[34] S. Zafary, A Single Term Formula for Approximating the Circumference of an Ellipse, (n.d.).

[35] S. Gabriel, R.W. Lau, C. Gabriel, The dielectric properties of biological tissues: II. Measurements in the frequency range 10 Hz to 20 GHz, Phys. Med. Biol. 41 (11) (1996) 2251–2269, https://doi.org/10.1088/0031-9155/41/11/002.

[36] A.O. Bah, P.-Y. Qin, R.W. Ziolkowski, Y.J. Guo, T.S. Bird, A Wideband Low-Profile Tightly Coupled Antenna Array With a Very High Figure of Merit, IEEE Trans. Antennas Propag. 67 (4) (2019) 2332–2343, https://doi.org/10.1109/TAP.2019.2891460.

[37] B.P. Nadh, B.T.P. Madhav, M.S. Kumar, Design and analysis of dual band implantable DGS antenna for medical applications, Sādhanā 44 (2019) 131, https://doi.org/10.1007/s12046-019-1099-8.

[38] M. Padmanabharaju, B.T.P. Madhav, D.S. Phani Kishore, P.V. Datta Prasad, Conductive fabric material based compact novel wideband textile antenna for wireless medical applications, Mater. Res. Express 6 (8) (2019) 086327, https://doi.org/10.1088/2053-1591/ab09a1.

[39] B. Prudhvi Nadh, B.T.P. Madhav, M. Siva Kumar, T. Anilkumar, M. Venkateswara Rao, P.V.V. Kishore, Windmill-shaped antenna with artificial magnetic conductor-backed structure for wearable medical applications, Int. J. Numer. Model. Electron. Networks Devices Fields 33 (6) (2020), https://doi.org/10.1002/jnm.2757.